Neurobiology of Disease 126 (2019) 23–35

Contents lists available at ScienceDirect

Neurobiology of Disease

journal homepage: www.elsevier.com/locate/ynbdi

Differences in structural and functional networks between young adult and aged rat brains before and after stroke lesion simulations

Milou Straathof[a,*,1], Michel R.T. Sinke[a,1], Annette van der Toorn[a], Paul L. Weerheim[a], Willem M. Otte[a,b], Rick M. Dijkhuizen[a]

[a] Biomedical MR Imaging and Spectroscopy Group, Center for Image Sciences, University Medical Center Utrecht and Utrecht University, Utrecht, the Netherlands
[b] Department of Pediatric Neurology, Brain Center Rudolf Magnus, University Medical Center Utrecht, Utrecht, the Netherlands

ARTICLE INFO

Keywords:
Aging
Diffusion MRI
Functional MRI
Graph theory
Lesion simulation
Network analysis
Rat brain
Stroke

ABSTRACT

Neural network changes during aging may contribute to vulnerability and resilience to brain lesions in age-related neurological disorders, such as stroke. However, the relationship between age-related neural network features and stroke outcome is unknown. Therefore, we assessed structural and functional network status in young adult and aged rat brain, and measured the effects of simulated stroke lesions.

Eleven rats underwent diffusion-weighted MRI and resting-state functional MRI at young adult age (post-natal day 88) and old age (between post-natal day 760 and 880). Structural and functional brain network features were calculated from graph-based network analysis. We performed three lesion simulations based on the brain injury pattern in frequently applied rodent stroke models, i.e. a small cortical lesion, a subcortical lesion, or a large cortical plus subcortical lesion, for which we computationally removed the involved network regions.

Global network characteristics, i.e. integration and segregation, were not significantly different between the two age groups. However, we detected local differences in structural and functional networks between young adult and old rats, mainly reflected by shifts of hub regions. Stroke lesion simulations induced significant global and local network changes, characterized by lower efficiency and shifts of hub regions in structural and functional networks, which was most evident after a large cortical plus subcortical lesion. Functional and structural hub region shifts after lesion simulations differed between young adult and aged rats.

Our lesion simulation study demonstrates that age-dependent brain network status affects structural and functional network reorganization after stroke, particularly involving hub shifts, which may influence functional outcome. Computational lesion studies offer a cheap and simple alternative to empirical studies and can complement or guide more complicated experimental studies in animal models and patients.

1. Introduction

Stroke – i.e. a sudden loss of blood flow to the brain – is one of the main causes of long-term disability in adults, and affects almost 17 million people worldwide per year (Feigin et al., 2014). Despite the significant functional consequences, many patients show (partial) recovery of sensorimotor and cognitive functions during the weeks and months following stroke, which may be related to reorganization of surviving networks in the brain (Cramer, 2008; Grefkes and Fink, 2011; Jiang et al., 2013; Jones, 2017; Murphy and Corbett, 2009). Post-stroke brain remodeling occurs at different levels and locations, i.e. from micro- (e.g. synaptic plasticity) to macro-scale (e.g. cortical remapping) (Biernaskie and Corbett, 2001; Jones et al., 1996; Stroemer et al., 1995) and from peri- to contralesional sites (Cai et al., 2016; Crofts et al., 2011; Dacosta-Aguayo et al., 2014; Granziera et al., 2012; Gratton et al., 2012; Johansen-Berg et al., 2010; Schaechter et al., 2009), respectively. These insights have led to the notion that assessment of neural networks at whole-brain level is critical for optimal understanding of the functional consequences of stroke (Carter et al., 2012; Grefkes and Fink, 2011; Rehme and Grefkes, 2013).

Brain networks consist of spatially distributed regions that are connected and interacting with each other at micro-, meso- and macro-scales (Bassett and Sporns, 2017; Bullmore and Sporns, 2009). Modern network science describes the brain as a collection of nodes (e.g.

* Corresponding author at: Biomedical MR Imaging and Spectroscopy Group, Center for Image Sciences, University Medical Center Utrecht and Utrecht University, Heidelberglaan 100, 3584 CX Utrecht, the Netherlands.
E-mail address: M.Straathof-2@umcutrecht.nl (M. Straathof).
[1] Shared first author.

https://doi.org/10.1016/j.nbd.2018.08.003
Received 30 April 2018; Received in revised form 17 July 2018; Accepted 3 August 2018
Available online 04 August 2018
0969-9961/

individual neurons, neuronal clusters or functional brain regions) and edges or ties (e.g. structural or functional connections between nodes). A healthy brain's network topology is described by an optimal balance between integration (i.e. global efficiency) and segregation (i.e. local specialization) of neural signaling, characterized by small-world organization, modularity and a 'rich club' of highly connected hub regions (Bassett and Bullmore, 2009; Bassett and Sporns, 2017; Bullmore and Sporns, 2009; Sporns, 2010). These topological characteristics have been found across species (van den Heuvel et al., 2016a, 2016b, 2015) and deviation from optimal organization has been observed in relation to aging, brain dysfunction and cerebral injury, including stroke (Bassett and Bullmore, 2009; Bullmore and Sporns, 2009; Sporns, 2010; Stam, 2014; van Meer et al., 2012). Moreover, network changes during aging may contribute to vulnerability and resilience to brain lesions in age-related neurological disorders, such as stroke. However, the relationship between age-related neural network features and stroke is largely unknown. Systematic studies on this relationship in stroke patients are complicated and may be more straightforwardly conducted in laboratory rodents that age relatively fast and can be scanned serially in a fairly short time-frame.

Experimental animal stroke studies are generally performed in young adult rodents, even though the risk and prevalence of human stroke is higher at older age. Recently, this age discrepancy between animal stroke models and human stroke patients has been put forward as one of the causes of poor bench-to-bedside translation (Dirnagl, 2016). The age at which stroke is induced is known to influence stroke outcome and response to therapies in experimental models (Liang et al., 2016; Herson and Traystman, 2014; Liu et al., 2009). In the current study, we aimed to identify differences in brain networks of young adult and aged rats as well as their susceptibility and resilience to stroke lesions. We used data from rats that were longitudinally scanned with MRI from early adulthood to old age. The imaging protocol included resting-state functional MRI (resting-state fMRI) and diffusion MRI, which allowed assessment of large-scale functional and structural neural network status under healthy conditions. We simulated lesions in brain areas that are typically affected in different rodent stroke models, i.e. cortical photothrombosis (Watson et al., 1985), short transient middle cerebral artery occlusion (MCAO), and permanent or long transient MCAO (Garcia et al., 1995; Li et al., 1995). In addition, we simulated lesions in a single hub region and in a single non-hub region to measure their effect on the global network characteristics. We chose regions that are normally not affected in the abovementioned stroke models. We hypothesized that local and global network characteristics alter in relation to lesion extent, and that this relationship differs between young adult and aged rats.

2. Materials and methods

2.1. Animals

Twenty healthy male Wistar rats (Harlan, Horst, The Netherlands) were housed in groups of four rats per cage. The rats had ad libitum access to food and water, were housed with a light/dark cycle of 12 h (lights on at 7:00 AM), and temperature was controlled between 22 and 24 °C. All experiments were approved by the committee for Animal Experiments of the University Medical Center Utrecht, The Netherlands (protocol number 2010.I.10.228), and were performed in accordance with the guidelines of the European Communities council directive.

MRI was done at multiple time-points during the lifespan of the rats, until their natural death. We analyzed data from eleven animals that were scanned during early adulthood (postnatal day 88), i.e. comparable to the age of rats in most preclinical stroke studies, as well as at old age (postnatal day 760 or 880), i.e. representative of the age during which clinical stroke is prevalent. Scans from animals that died before this age were not included in the analyses.

2.2. MRI acquisition

MRI experiments were conducted on a 4.7 T horizontal bore MR system. We used a homebuilt Helmholtz volume coil (90 mm diameter) and an inductively coupled surface coil (25 mm diameter) for signal excitation and detection, respectively. Rats were anesthetized with 4% isoflurane and endotracheally intubated for mechanical ventilation (TOPO, Kent Scientific, Torrington, CT, USA) with 1–2% isoflurane in a mixture of air with 30% O_2 (55 breaths per minute). Rats were subsequently immobilized in a specially designed MR-compatible stereotactic holder, including earplugs and a tooth holder. During MRI, end-tidal CO_2 as well as blood oxygen saturation and heart rate were continuously monitored with a capnograph (Multinex 4200, Datascope Corporation, Paramus, NJ, USA) and pulse oximeter (8600 V, Nonin Medical, Plymouth, MN, USA), respectively. Body temperature was maintained at 37.0 ± 0.5 °C.

For resting-state fMRI, T_2*-weighted blood oxygenation level-dependent (BOLD) images were acquired under 1.0% isoflurane anesthesia, with a ventilation-triggered single-shot 3D gradient-echo echo planar imaging (EPI) sequence (repetition time (TR)/echo time (TE) = 32/19 ms (effective TR = 1.024 s); 12° pulse angle; field-of-view (FOV) = 32 × 24 × 12 mm^3; 64 × 48 × 32 acquisition matrix; 0.5 × 0.5 × 0.5 mm^3 voxels; 600 BOLD images in approximately 10 min). Diffusion MRI was executed under 1.5–2.0% isoflurane with a 2D 5-shot EPI sequence (TR/TE = 1750/28.52 ms; 4 b_0 images, 4 b-values (650, 1285, 1919 and 2518 s/mm^2); δ/Δ = 5/10 ms; 30 directions per b-value, three averages; 128 × 128 acquisition matrix; 0.195 × 0.195 mm^2 voxels; 19 1.0-mm slices). In addition, anatomical images were acquired with a 3D gradient-echo sequence (TR/TE = 6/2.25 ms; 40° flip angle; 4 averages; FOV = 40 × 25 × 20 mm^3; 160 × 100 × 80 matrix; 0.25 × 0.25 × 0.25 mm^3 voxels).

2.3. Image processing

2.3.1. Resting-state functional connectivity

Resting-state functional MR images were processed with FSL 5.0 (Jenkinson et al., 2012), unless otherwise stated. Preprocessing steps of the resting-state fMRI scans included removal of the first 10 images to reach a steady state, motion-correction with *MCFLIRT* (Jenkinson et al., 2002) and brain-extraction with *BET* (Smith, 2002). Motion-correction parameters were used as regressors for the resting-state signal (no linear detrending and global mean regression were performed). Low-frequency BOLD fluctuations were obtained by applying temporal filtering between 0.01 and 0.1 Hz in *AFNI* (Cox, 1996). We calculated Fisher's *Z*-transformed correlation coefficients to measure inter- and intrahemispheric functional connectivity between regions-of-interest (ROIs) (see below). Individual functional connectivity matrices were divided by their own mean to correct for individual differences in mean functional connectivity strength. This procedure is based on a normalization step in the analysis of structural networks described by van den Heuvel et al. (2010). They reported normalization by dividing all network edge values by the maximum network edge value. However, since many functional connectivity networks in our study were skewed towards lower correlation values with high value outliers (see Supplementary Fig. 1), we normalized functional network values with the mean rather than the maximum value. For comparison, we performed a sensitivity analysis with the maximum value as normalization factor and data are presented in Supplementary Figs. 2–5. Results were highly similar between mean and maximum normalization procedures.

2.3.2. Diffusion-based structural connectivity

Diffusion-weighted images were preprocessed with FSL 5.0 (Jenkinson et al., 2012) and MRtrix3 (Tournier et al., 2012). Motion and eddy current corrections were done with *dwipreproc* (MRtrix3), which uses FSL tools (Andersson and Sotiropoulos, 2016). Calculation of diffusion parameters, i.e. fractional anisotropy (FA), mean diffusivity

(MD), axial diffusivity (AD) and radial diffusivity (RD), was done with *dtifit* in FSL.

Further processing, tractography and connectome reconstruction were done in MRtrix3. We first determined multi-shell response functions for white matter (WM), grey matter (GM) and cerebral spinal fluid (CSF) using *dwi2response* and custom-made WM, GM and CSF masks. Multi-shell multi-tissue constrained spherical deconvolution (CSD) (Jeurissen et al., 2014) was performed to generate WM, GM and CSF volume fraction maps, and to obtain fiber orientation distribution (FOD) maps for WM, GM and CSF separately, of which the WM FOD map was used for tractography.

We performed CSD tractography using the iFOD2 algorithm (Tournier et al., 2010), with dynamic seeding over the WM FOD map, a step-size of 0.1 mm, an angle threshold of 45° and an FOD amplitude threshold of 0.2, thereby generating 1 million tracts over the entire brain. After whole-brain tractography we used Spherical deconvolution Informed Filtering of Tractograms (SIFT) to improve the accuracy of the reconstructed whole-brain connectome by fitting and optimizing tracts at whole-brain level to the underlying diffusion-weighted images, and by removing (i.e. filtering) inappropriate tracts from the connectome (Smith et al., 2015, 2013).

Whole-brain structural networks were constructed by matching the filtered tracts with ROIs in subject space. Two regions were considered connected if one or more tracts traversed – or had their endpoints in – both regions. The streamline count after SIFT was used as measure of structural connectivity strength.

2.3.3. Regions-of-interest

After preprocessing, resting-state fMRI and diffusion MRI images were linearly and non-linearly registered to a reference rat brain using *FLIRT* and *FNIRT* (Andersson et al., 2007; Jenkinson and Smith, 2001), respectively. The reference rat brain was aligned with a custom-built 3D reconstruction of the Paxinos and Watson rat brain atlas (Majka et al., 2012; Paxinos and Watson, 2005). We included 88 cortical and subcortical regions from the atlas, covering most of the rat brain, with sufficient assurance of spatial alignment (i.e. inclusion of at least 8 voxels per ROI in the resting-state scans)(See Table 1). Subsequently, all ROIs were back-projected in subject space, where further analyses were performed.

2.4. Graph-based network analysis

To determine the effects of lesion simulations on global and local network characteristics of structural and functional brain networks, we used graph analyses (Bullmore and Sporns, 2009). These graph analyses were performed on individual weighted networks, for resting-state fMRI and diffusion MRI networks separately. A weighted graph G = (V,W) was constructed with V as the collection of all included regions N, and W as the collection of all edge weights w. Self-connections were excluded, and negative edge weights in the functional weighted graphs were set to 0. The Fisher's *Z*-transformed correlation coefficient was used as functional edge weight, while the SIFT-corrected streamline count was used as structural edge weight. To characterize brain networks, we calculated global as well as local network parameters separately.

2.4.1. Global parameters

To characterize the network topology we measured several global network parameters: the weighted-undirected clustering coefficient (C) (Fagiolo, 2007) as a measure of segregation, the weighted shortest path length (L) (Stam et al., 2009), as a measure of global efficiency or integration, and the small-worldness (Humphries and Gurney, 2008). All global parameters were calculated for structural and resting-state functional networks.

- **Clustering coefficient (C)**: The weighted clustering coefficient provides a measure of the degree to which the nearest neighbors of each node are directly connected to each other. It sums the weights of the connections that exist between the nearest neighbors, divided by the potential maximum number of connections in triplets of nodes. We first calculated the weighted C for each node i in the entire graph:

$$C_i = \frac{\sum_{j\neq i}\sum_{h\neq(i,j)} w_{ij}^{\frac{1}{3}} w_{ih}^{\frac{1}{3}} w_{jh}^{\frac{1}{3}}}{d_i(d_i-1)}$$

In which d_i is the number of connections of node i. This equation considers weights of all edges in a triplet and excludes weights that are not participating in a triplet. Subsequently, the weighted C was determined by taking the mean of the local clustering coefficients over all the nodes in the network:

$$C = N^{-1}\sum_{i=1}^{N} C_i$$

- **Weighted shortest path length (L):** The weighted shortest path length provides a measure of the average minimal distance between a node and all the other nodes in the network. This is measured as the inverse of the weights of the connections that have to be crossed to go from one node to another. We first calculated the weighted path length (l_{ij}^{w}) for each pair of nodes (i and j) in the entire graph using Dijkstra's algorithm for weighted graphs (Dijkstra, 1959), by taking the minimum sum of the inverse weights (d_{ij}) to travel between node i and j:

$$l_{ij}^{w} = min_{i\leftrightarrow j}(sum(d_{ij}))and\ d_{ij} = 1/w_{ij}$$

To handle disconnected edges, characterized by an infinite path length, we used the harmonic mean ($1/\infty \rightarrow 0$). The harmonic mean takes the reciprocal of the mean of the reciprocals (Newman, 2003):

$$L = N(N-1)\Big/\sum_{i=1,j\neq i}^{N}\frac{1}{l_{ij}^{w}}$$

- For each functional and structural network, C and L were normalized based on 10 randomly rewired surrogate networks (Maslov and Sneppen, 2002). The normalized weighted clustering (γ) and path length (λ) were defined as:

$$\gamma = \frac{C}{C_{random}}\quad \lambda = \frac{L}{L_{random}}$$

- **Small-worldness** was calculated as a measure of the optimal balance between segregation (clustering) and integration (path length), by γ/λ, according to Humphries and Gurney (2008).

2.4.2. Local parameters

To investigate local (i.e. nodal) characteristics of the network, we identified most important nodes, i.e. the hubs, in the network, by quantifying the strength (weighted version of degree) (Barrat et al., 2004) and betweenness centrality (Brandes, 2001; Freeman, 1977) for each node separately.

- **Strength (S):** The connection strength of a node is the sum of all the edge weights connected to that node. This provides a measure of the total nodal connectivity (strength). We calculated the strength of each node in the entire graph:

$$S_i = \sum_{j=1}^{N} w_{ij}$$

- **Betweenness centrality (C_B):** The weighted betweenness centrality

of a node provides a measure of the importance of the node in network connectivity. It measures the degree to which a node lies on the shortest path between two other nodes. We calculated the betweenness centrality for each node in the entire graph:

$$C_B(v) = \sum_{s \neq v \neq t \in V} \frac{\sigma_{st}(v)}{\sigma_{st}}$$

In this formula, $\sigma_{st}(v)$ is the number of shortest paths from s to t in which node v is partaking.

- **Hub nodes**, or hub regions, are regions in the brain with a central position, which play a crucial role in network communication. Hub regions can be defined by different metrics. They generally have a low clustering coefficient and shortest path length, and a high average strength and betweenness centrality (Bullmore and Sporns, 2009; Sporns et al., 2007). Therefore, we determined the hubs based on these four characteristics, as previously described (van den Heuvel et al., 2010). First, we averaged these four characteristics for each region over all individual rats at each time-point separately. Subsequently, we determined which regions belonged to the top 20% for each of the four characteristics separately (the regions with the 20% lowest clustering coefficients or path lengths, and/or the 20% highest strengths or betweenness centralities). When the node belonged to the top 20% for a category, the hub score for that category was one. Regions could get a hub score between 0 and 4, and hub regions were identified as regions with a hub score of 2 or higher.

2.5. Lesion simulations

To quantify effects of lesion simulations in young adult and aged rats, we simulated three different stroke lesion types that are typically observed in frequently applied rat stroke models (Fluri et al., 2015): small cortical lesions, subcortical lesions and large cortical plus subcortical lesions (see Fig. 1). Lesions were simulated by elimination of edges from the nodes that were selected as part of the lesion (i.e. structural and functional connections were set to 0). Subsequently, network parameters were calculated as described above, for each type of simulated stroke lesion in young adult and aged rats.

2.5.1. Small cortical lesion

A focal cortical lesion is a hallmark of the photothrombotic stroke model, which involves systemic injection of a photosensitive dye (Rose-Bengal) followed by focal illumination of the cortex through the intact skull (Watson et al., 1985). In the rat photothrombotic stroke model, lesion induction is often targeted to the forelimb area of the somatosensory cortex (S1FL). Therefore we modeled photothrombotic stroke by eliminating S1FL nodes in our functional and structural networks.

2.5.2. Subcortical lesion

Probably the most frequently applied rat stroke model involves unilateral occlusion of the middle cerebral artery (MCA) with an intraluminal filament (Longa et al., 1989). Short temporary (30–60 min) MCA occlusion usually results in subcortical damage in the caudate putamen (CPu), modeled in our study by eliminating the CPu node in functional and structural networks.

2.5.3. Large cortical plus subcortical lesion

Longer (60–120 min) or permanent MCA occlusion induces extensive cortical and subcortical damage. We simulated these large lesions by eliminating the CPu node and nodes representing all sub-regions of the primary somatosensory cortex (S1) (i.e. the forelimb region (S1FL) and hindlimb region (S1HL), jaw region (S1J), upperlip region (S1ULp), barrel field region (S1BF), trunk region (S1Tr) and the dysgranular zone of S1 (S1DZ)), the secondary somatosensory cortex (S2), and the insular cortex (i.e. AID, AIP, AIV, DI and GI).

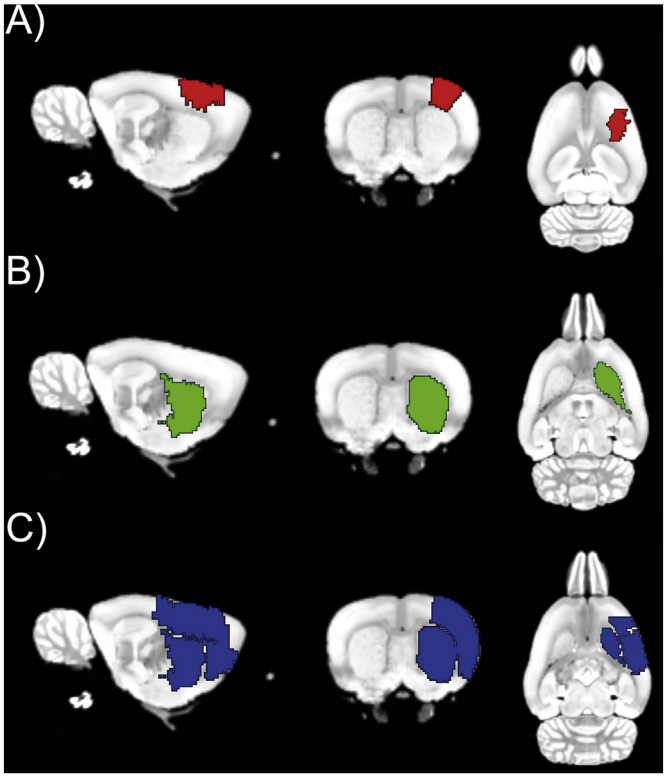

Fig. 1. Lesion simulations. Regions overlaid on a sagittal (left), coronal (middle) and transversal (right) rat brain slice indicate typical lesion areas after cortical photothrombotic stroke (A (red)), and short (B (green)) or long (C (blue)) middle cerebral artery occlusion. Simulated lesion areas involved multiple slices throughout the brain, but are here displayed on a single slice in each plane for illustration purposes. (For interpretation of the references to colour in this figure legend, the reader is referred to the web version of this article.)

2.5.4. Lesions in a single hub or non-hub region

We simulated lesions in two additional areas: (1) the right hippocampus, a hub region in both structural and functional networks in young adult and aged rats, and (2) the right medial parietal association cortex, a non-hub region in all networks.

2.6. Statistical analyses

To statistically determine whether global and local network characteristics differed between healthy young adult and aged rats, we performed paired t-testing for each global and nodal parameter. Because local characteristics were determined for 88 regions-of-interest, we corrected the nodal analyses for multiple testing using a false-discovery rate (FDR) correction (Benjamini and Hochberg, 1995). Comparisons with p-values lower than 0.05 after FDR correction were considered statistically significantly different. To test for homotopic symmetrical hubs, i.e. whether homotopic regions in the left and right hemispheres both belonged to the hub regions, we calculated the Dice index (Yin and Yasuda, 2006) for homotopic hub regions in young adult and aged rats separately.

To assess the effect of simulated stroke lesions, we calculated the difference value for each global or nodal characteristic between the healthy condition and lesion simulation: $value_{\Delta} = value_{lesioned\ network} - value_{healthy\ network}$. To measure the effect of a lesion on network characteristics, we first tested whether the network parameters changed significantly compared to the healthy condition with a one sample t-test for each simulated lesion type at each age separately. In addition, we compared the effects of different stroke lesion simulations on the

Table 1
Included regions-of-interest for resting-state fMRI and diffusion MRI analyses.

Names (abbreviations) of Paxinos & Watson atlas regions
Left and Right Agranular insular cortex dorsal part (AID)
Left and Right Agranular insular cortex posterior part (AIP)
Left and Right Agranular insular cortex ventral part (AIV)
Left and Right Primary auditory cortex (Au1)
Left and Right Secondary auditory cortex dorsal area (AuD)
Left and Right Secondary auditory cortex ventral area (AuV)
Left and Right Cingulate cortex area 1 (Cg1)
Left and Right Cingulate cortex area 2 (Cg2)
Left and Right Dysgranular insular cortex (DI)
Left and Right Dorsolateral entorhinal cortex (DLEnt)
Left and Right Ectorhinal cortex (Ect)
Left and Right Frontal cortex area 3 (Fr3)
Left and Right Frontal association cortex (FrA)
Left and Right Granular insular cortex (GI)
Left and Right Lateral orbital cortex (LO)
Left and Right Lateral parietal association cortex (LptA)
Left and Right Primary motor cortex (M1)
Left and Right Secondary motor cortex (M2)
Left and Right Medial parietal association cortex (MptA)
Left and Right Perirhinal cortex (Prh)
Left and Right Retrospenial dorsal (RSD)
Left and Right Retrosplenial granular cortex a region (RSGa)
Left and Right Retrosplenial granular cortex b region (RSGb)
Left and Right Primary somatosensory cortex barrel field (S1BF)
Left and Right Primary somatosensory cortex dysgranular region (S1DZ)
Left and Right Primary somatosensory cortex forelimb region (S1FL)
Left and Right Primary somatosensory cortex hindlimb region (S1HL)
Left and Right Primary somatosensory cortex jaw region (S1J)
Left and Right Primary somatosensory cortex trunk region (S1Tr)
Left and Right Primary somatosensory cortex upper lib region (S1ULp)
Left and Right Secondary somatosensory cortex (S2)
Left and Right Temporal association cortex 1 (TeA)
Left and Right Primary visual cortex (V1)
Left and Right Primary visual cortex binocular area (V1B)
Left and Right Primary visual cortex monocular area (V1M)
Left and Right Secondary visual cortex lateral area (V2L)
Left and Right Secondary visual cortex mediolateral area (V2ML)
Left and Right Secondary visual cortex mediomedial area (V2MM)
Left and Right Ventral orbital cortex (VO)
Left and Right Thalamus (T)
Left and Right Globus Pallidum (GP)
Left and Right Caudate putamen (CPu)
Left and Right Accumbens nucleus (Acc)
Left and Right Hippocampus (Hipp)

network parameters with an ANOVA for each age separately. Secondly, we evaluated for each simulated lesion type, whether the lesion-induced change in network parameters differed between young adult and aged rats using a paired *t*-test. In addition, we calculated the Dice index for the hub regions in structural and functional networks before (healthy condition) and after each type of simulated lesion for young adult and aged rats separately.

We constructed 95% confidence intervals for the Dice indices by means of bootstrapping. This involves repeated calculation of the Dice indices on 10.000 resampled sets, with replacement (Bland and Altman, 2015). Subsequently, we used bootstrapping to construct 95% confidence interval of delta Dice indices. To test whether the homotopic organization of hubs, as well as hub shifts after the simulated lesions, were significantly different between young and old rats we determined p-values from the 95% confidence intervals (Altman and Bland, 2011).

3. Results

3.1. Aging effects

3.1.1. Stable global structural and functional network features between young adulthood and old age

Fig. 2 shows quantitative results from the graph-based whole-brain network analyses of functional connectivity and structural tractography

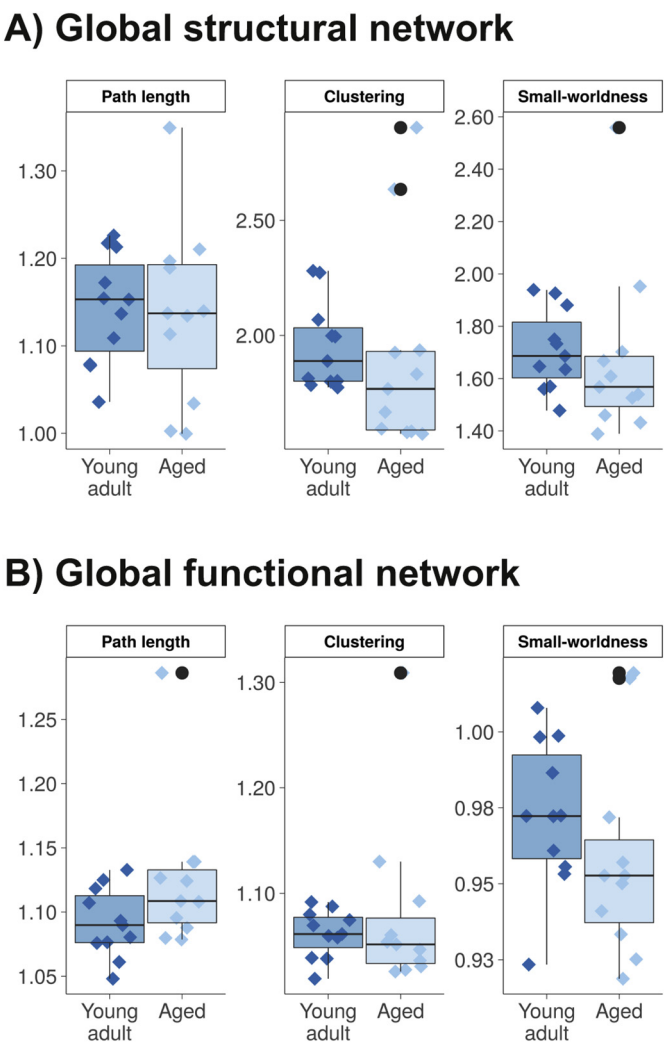

Fig. 2. Global network parameters for whole-brain structural and resting-state functional networks in young adult and aged rats. Path length, clustering coefficient and small-worldness in (A) diffusion MRI-based whole-brain structural networks and (B) resting-state fMRI-based whole-brain functional networks in young adult (dark blue) and aged rats (light blue). Individual values are shown as diamonds with horizontal jitter for visualization purposes. Boxplots show median and inter-quartile range (IQR), whiskers representing 1.5 times the IQR, and dots representing outliers. Outliers are defined as values exceeding 1.5 times the IQR above the upper and below the lower quartile. Clustering = Clustering coefficient. (For interpretation of the references to colour in this figure legend, the reader is referred to the web version of this article.)

data from young adult and aged rats. For structural (Fig. 2A) as well as resting-state functional networks (Fig. 2B), we found no significant differences in global network measures, i.e. clustering coefficient, path length and small-worldness, between young adult and aged rats.

3.1.2. Higher nodal strength in structural network of aged rats

To investigate local network features in the rat brain, we calculated the nodal strength and betweenness centrality for each region-of-interest in the structural and resting-state functional networks. We found statistically significant differences in node strength between young adult rats and aged rats for several regions in the structural network, which are listed Table 2. In all these regions node strength – and betweenness centrality for the right frontal area 3, left cingulum area 2 and left lateral orbital cortex – was increased at old age, except for the left dysgranular insular cortex, which showed decreased betweenness centrality.

Table 2
Regions with significantly altered nodal network measures in aged rats compared to young adult rats.

Region of interest	*Nodal network feature*	*Δ Percentage*	*FDR corrected P-value*
Left Acc	Strength	80	< 0.01
Right Acc	Strength	100	< 0.01
Left AID	Strength	111	< 0.01
Right AID	Strength	111	< 0.01
Right AIP	Strength	88	0.02
Left AIV	Strength	167	< 0.001
Right AIV	Strength	184	< 0.001
Right AuV	Strength	75	0.04
Left Cg1	Strength	119	< 0.001
Right Cg1	Strength	85	< 0.01
Left Cg2	Betweenness	237	0.04
Left Cg2	Strength	65	< 0.01
Right Cg2	Strength	58	< 0.01
Left CPu	Strength	45	< 0.01
Right CPu	Strength	55	< 0.01
Left DI	Betweenness	−33	0.04
Right DI	Strength	88	< 0.01
Left Fr3	Strength	147	< 0.001
Right Fr3	Betweenness	84	0.02
Left FrA	Strength	1088	< 0.01
Left GP	Strength	43	0.02
Right GP	Strength	74	< 0.01
Left LO	Betweenness	172	0.03
Left LO	Strength	293	< 0.001
Right LO	Strength	193	< 0.001
Left M1	Strength	65	< 0.01
Right M1	Strength	105	< 0.001
Left M2	Strength	89	< 0.01
Right M2	Strength	125	< 0.01
Right MptA	Strength	82	0.02
Right Prh	Strength	50	0.02
Right RSGb	Strength	44	0.03
Right S1BFa	Strength	35	< 0.01
Right S1J	Strength	60	0.04
Left T	Strength	55	< 0.01
Right T	Strength	78	< 0.01
Left V1	Strength	60	0.02
Left V2ML	Strength	142	0.04
Right V2MM	Strength	102	0.04
Left VO	Strength	181	< 0.001
Right VO	Strength	170	< 0.001

In contrast, there were no statistically significant differences in strength or betweenness centrality of the functional network nodes between young adult and aged rats.

3.1.3. Network hub nodes shift between young adulthood and old age

Hub nodes, i.e. the nodes with the highest degree of connectivity within the network, characterized by a low clustering coefficient and short path length, and a high strength and betweenness centrality, were found throughout the rat brain. The distribution of hub nodes in the structural brain network is shown in Fig. 3A for young adult and aged rats. Consistent hub nodes in young adult and aged rats were, for example, the left and right caudate putamen and hippocampi. From young adulthood to old age, several regions (e.g. in the left somatosensory cortex) appeared to lose their hub status, whereas other regions (e.g. the left and right primary and secondary motor cortices) acquired a hub status. In aged rats, hubs tended to be more symmetrically distributed in bilateral homotopic areas (e.g., the left and right primary and secondary motor cortices, caudate putamen, and dorsolateral entorhinal cortices), and were located more medially as compared to young adult rats. The overlap in hub nodes in the young adult and aged structural network, expressed by the Dice coefficient was 0.29 (95% CI = 0.14–0.44). The Dice coefficient reflecting the overlap between hub regions in the left and right hemispheres was 0.61 (95% CI = 0.31–0.85) for aged rats, compared to 0.32 (95% CI = 0.11–0.53) for young adult rats (ΔDice = 0.30, 95% CI = −0.03–0.62, p = .13).

The distribution of hub nodes in the resting-state functional network (Fig. 3B) was different from that in the structural network. Nevertheless, consistent with the findings in the structural network, the left and right caudate putamen and hippocampi were also hub nodes in the functional networks of young adult and aged rats. There was a relatively higher density of functional network hub nodes in posterior and temporal regions (such as the temporal association area and perirhinal cortex) in aged rats as compared to young adult rats. The overlap in hub nodes in the young adult and aged functional network never reached 1 (mean Dice: 0.53; 95% CI = 0.37–0.68). Regions that lost their hub status in the resting-state functional network in aged rats included the right insular cortex, while other regions, such as the bilateral thalamus, acquired hub status. In line with the structural network hubs, functional network hub nodes in old rats tended to be more symmetrically distributed in homotopic areas in the left and right hemispheres. The Dice coefficient (reflecting the overlap between hub regions in the left and right hemisphere) was 0.61 (95% CI = 0.39–0.83) for old rats, compared to 0.53 (95% CI = 0.32–0.74) for young adult rats (ΔDice = 0.08, 95% CI = −0.14 - 0.32, p = .44).

3.2. Lesion simulations

To determine the effect of stroke lesions on network parameters in young adult and old rats, we simulated the extent of network damage for different frequently applied stroke models (cortical photothrombosis, transient MCAO with only subcortical damage, and transient/permanent MCAO with cortical and subcortical damage). We calculated a delta-score for each network parameter as the change in the network parameter after lesion simulation as compared to the parameter for the healthy network.

3.2.1. Unilateral stroke lesion simulations affect global structural and functional network features at a whole-brain level

The effect of stroke lesion simulations on global structural network characteristics are shown in Fig. 4A. Subtle, but statistically significant changes were measured after cortical (i.e. increased clustering ($p < .01$)) and subcortical stroke simulations (i.e. increased path length and decreased small-worldness ($p < .01$)), which were comparable between young adult and old aged rats. Subcortical plus cortical damage resulted in considerable increases in path length and clustering in both age groups ($p < .01$).

For whole-brain functional networks, stroke lesion simulations resulted in significant changes for all measured global network characteristics, i.e. increased path length, higher clustering and lower small-worldness ($p < .01$; Fig. 4B). These changes were relatively small for the cortical and subcortical stroke simulations, and substantial for the large stroke lesions involving cortical plus subcortical regions. There were no significant differences in these global functional network changes between young adult and aged animals.

Additional analyses of lesion simulations in the right hippocampus (hub region) or right medial parietal association cortex (non-hub region) revealed subtle but significant effects on structural and functional networks, which were highly comparable with the effects of cortical stroke and sub-cortical stroke (Suppl. Fig. 6).

3.2.2. Hub regions shift after stroke simulations

In addition to changes in global network features, stroke lesion simulations resulted in shifts of hub nodes in young adult and aged rats' structural and functional networks (Figs. 5 and 6). These shifts were most apparent after simulation of a large cortical plus subcortical lesion. In structural networks, some regions acquired a hub status, whereas other regions lost their hub status after lesion simulations (Fig. 5). In functional networks, regions mainly acquired a hub status after lesion simulations (Fig. 6). The number of regions with shifted hub status was higher in structural networks than in functional networks, which was indicated by a lower Dice coefficient for the overlap in hub

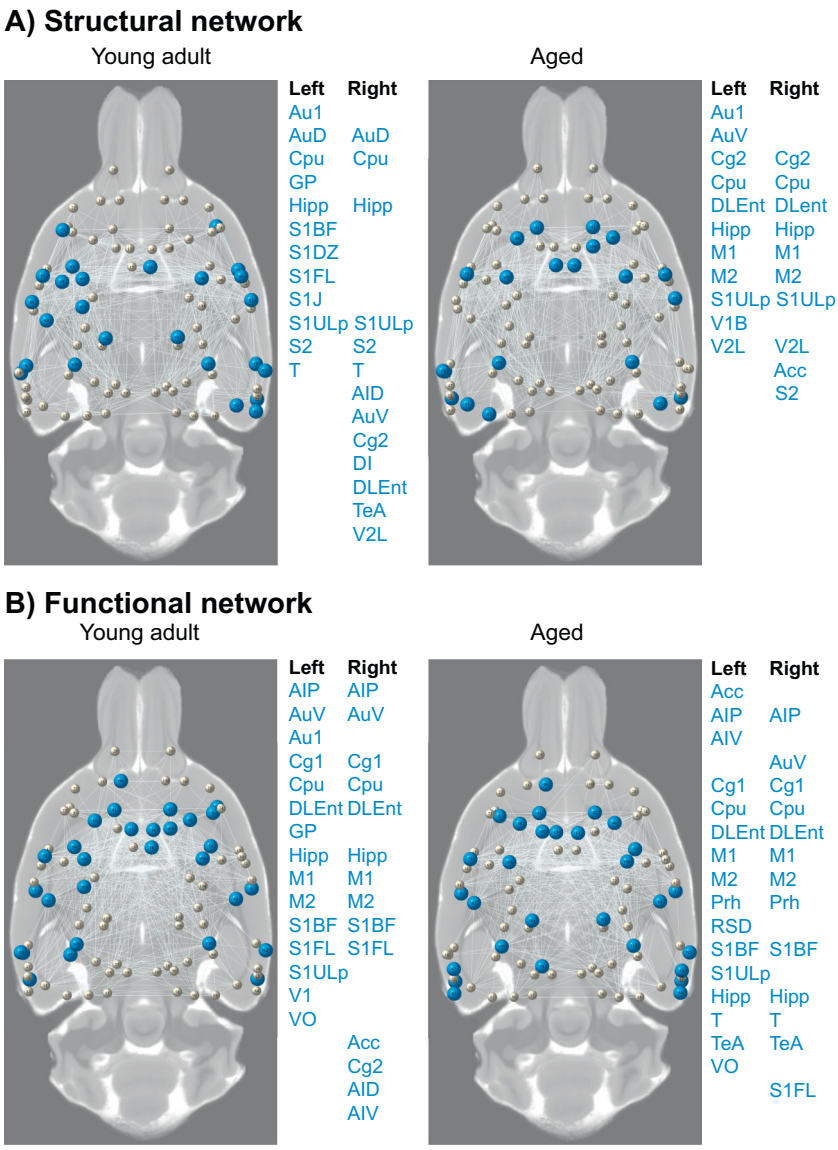

Fig. 3. Hub regions in structural and functional whole-brain networks in young adult and aged rats. Hub regions in (A) structural networks and (B) resting-state functional networks, overlaid on an axial structural MR image of a rat brain slice, are displayed in the 3D network as large blue nodes, whereas the other (non-hub) regions are presented as small white nodes. Networks are shown for young adult (left) and aged rats (right). Hub regions are listed right from the maps. (For interpretation of the references to colour in this figure legend, the reader is referred to the web version of this article.)

regions before and after stroke simulation (Table 3).

As can be observed in Figs. 5 and 6, there were several local differences between young adult and old rats in the pattern of shifts in hub regions in structural and functional networks after stroke simulations. For example, in aged rats we found that the left, contralesional forelimb region of the primary somatosensory cortex acquired a functional network hub status after a unilateral lesion in subcortical or cortical plus subcortical tissue, which was not observed in young adult rats.

4. Discussion

In this study, we investigated whether the effects of simulated lesions – representing topographical profiles of different rodent stroke models – on structural and functional network organization in rat brain differed between young adulthood and old age. Overall, global network features were largely comparable, however, local differences in structural and functional networks were observed between young adult and aged rats, particularly expressed by shifts in hub regions in the brain. Unilateral stroke simulations induced global changes in whole-brain structural and functional network organization, which was most significant for the large stroke simulation, involving cortical and subcortical lesioning. Global network changes after stroke simulations were comparable between young adult and aged rats. On the other hand, lesion-induced regional changes in hub status, which were more pronounced in the structural than in the functional brain network, differed between young adult and aged rats.

4.1. Whole-brain structural and functional networks – effects of aging

The measured similarity of global network characteristics between healthy young adult and aged rats, as measured from the path length, clustering and small-worldness in the structural and functional networks, is in line with human data. Small-world topology has been demonstrated in structural brain networks of young and aged adult humans (Gong et al., 2009; Zhu et al., 2012), and no aging effect was found for global network efficiency (Gong et al., 2009). However, other studies reported lower global efficiency in younger individuals (Wu et al., 2012; Zhu et al., 2012). This discrepancy may be explained by the

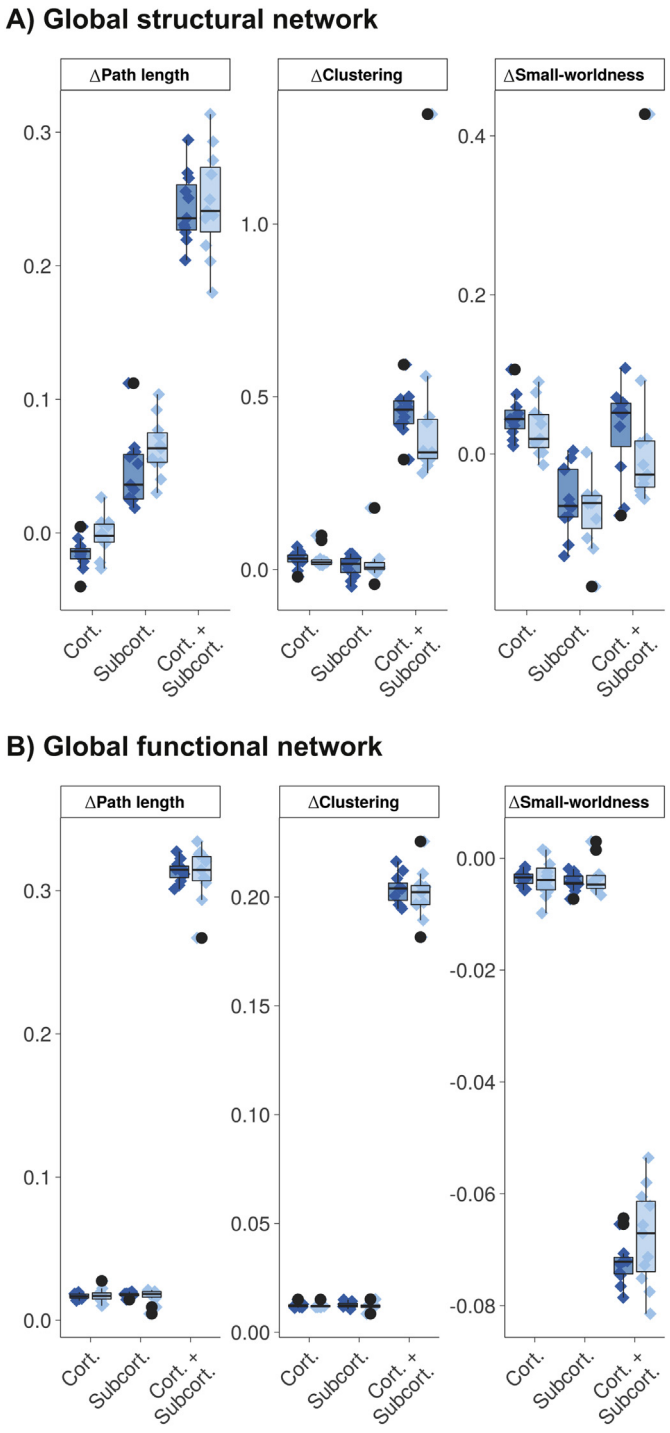

Fig. 4. Effects of different stroke lesion simulations on global network measures in young adult and old rats. Changes in path length, clustering and small-worldness after stroke lesion simulation, calculated as metric delta values between the healthy control network and the network after stroke simulation, for (A) diffusion-based structural networks and (B) resting-state fMRI-based functional networks. Delta-scores were determined for different stroke lesion simulations, i.e. cort: cortical (photothrombosis), subcort: subcortical (short transient MCAO) and cort + subcort: cortical plus subcortical (long transient or permanent MCAO), for young adult rats (dark blue) and aged rats (light blue). Individual values are given as diamonds with horizontal jitter for visualization purposes. Boxplots show median and inter-quartile range (IQR), whiskers representing 1.5 times the IQR, and dots representing outliers. Outliers are defined as values exceeding 1.5 times the IQR above the upper and below the lower quartile. (For interpretation of the references to colour in this figure legend, the reader is referred to the web version of this article.)

use of different age categories across studies. It has been demonstrated that global efficiency follows an inverted u-curve pattern between young and old age (Wu et al., 2012). Because the age groups in our study were at the extremities of this curve, we may have missed possible changes in global network characteristics that develop between the two time-points.

In functional networks, human resting-state fMRI studies have shown an increased minimum path length and clustering coefficient in older adults (Sala-Llonch et al., 2014). In addition, task-fMRI studies during memory encoding and recognition in healthy individuals demonstrated a similar increase in path length with aging (Wang et al., 2010). Although we did not find statistically significant aging effects on global networks, we did see a trend towards a higher path length and lower small-worldness in the functional network of old rats, resembling the described effects of aging in humans.

While global network features were largely the same, we identified local differences in structural and functional brain networks between young adult and aged rats. Node strength increased for many regions, such as the bilateral primary and secondary motor cortices and caudate putamen, within the whole-brain structural network, which seems in contrast to reductions in structural connectivity during aging as observed in humans (Gong et al., 2009). Loss of structural connectivity may be reflective of white matter degeneration in aging brains (Meier-Ruge et al., 1992; Salat et al., 2005). However, white matter degeneration may not be similarly prominent in aging rats. In fact, diffusion tensor imaging studies have revealed ongoing brain maturation in rats during adulthood (Mengler et al., 2014) with increasing fractional anisotropy in rodent white matter structures up to old age (Blockx et al., 2011). Furthermore, the mean diameter and volume density of myelinated fibers in the cortex are higher while the length density is lower, which may be explained by specific loss of thinner myelinated fibers, in aged as compared to younger adult rats (Zhang et al., 2009). These white matter differences can affect the diffusion-based tractography pattern and explain changes in node strengths that we observed between young adults and aged rats.

In addition to node strength differences in structural networks, we found shifts in hub regions from young adulthood to old age in structural and functional networks. Increased homotopical symmetry of hub regions in aged rats may be reflective of altered lateralization, which has also been reported for aged humans (Agcaoglu et al., 2015). Also, increasing homotopic connectivity with age, particularly between sensorimotor regions, has been found in a human resting-state fMRI study (Zuo et al., 2010). Moreover, similar to studies in human subjects, we observed a posterior shift in hub regions in the functional network, exemplified by hub status for the bilateral temporal association areas and perirhinal cortex in aged rats, although in humans this has been explained by lost hub status of frontal brain regions due to decreasing local network efficiency (Achard and Bullmore, 2007; Meunier et al., 2009).

4.2. Whole-brain structural and functional networks – effects of stroke lesion simulations

Computational lesion studies, as recently reviewed by Aerts et al. (2016), may substitute, complement or guide empirical studies in humans or animal models. Lesion simulation studies can be applied to already existing data, and provide a simple, cheap and non-invasive alternative to complicated longitudinal in vivo lesion studies, thereby contributing to replacement, reduction and refinement of animal research (Balls et al., 1995).

In the current study we simulated unilateral stroke lesions, based on lesion topographies of three popular rat stroke models. Additionally, we simulated focal lesions in a single hub (i.e. right hippocampus) or non-hub region (i.e. right medial parietal association cortex) region. Significant changes in global network features were measured in whole-brain structural and functional networks. Results from our in silico

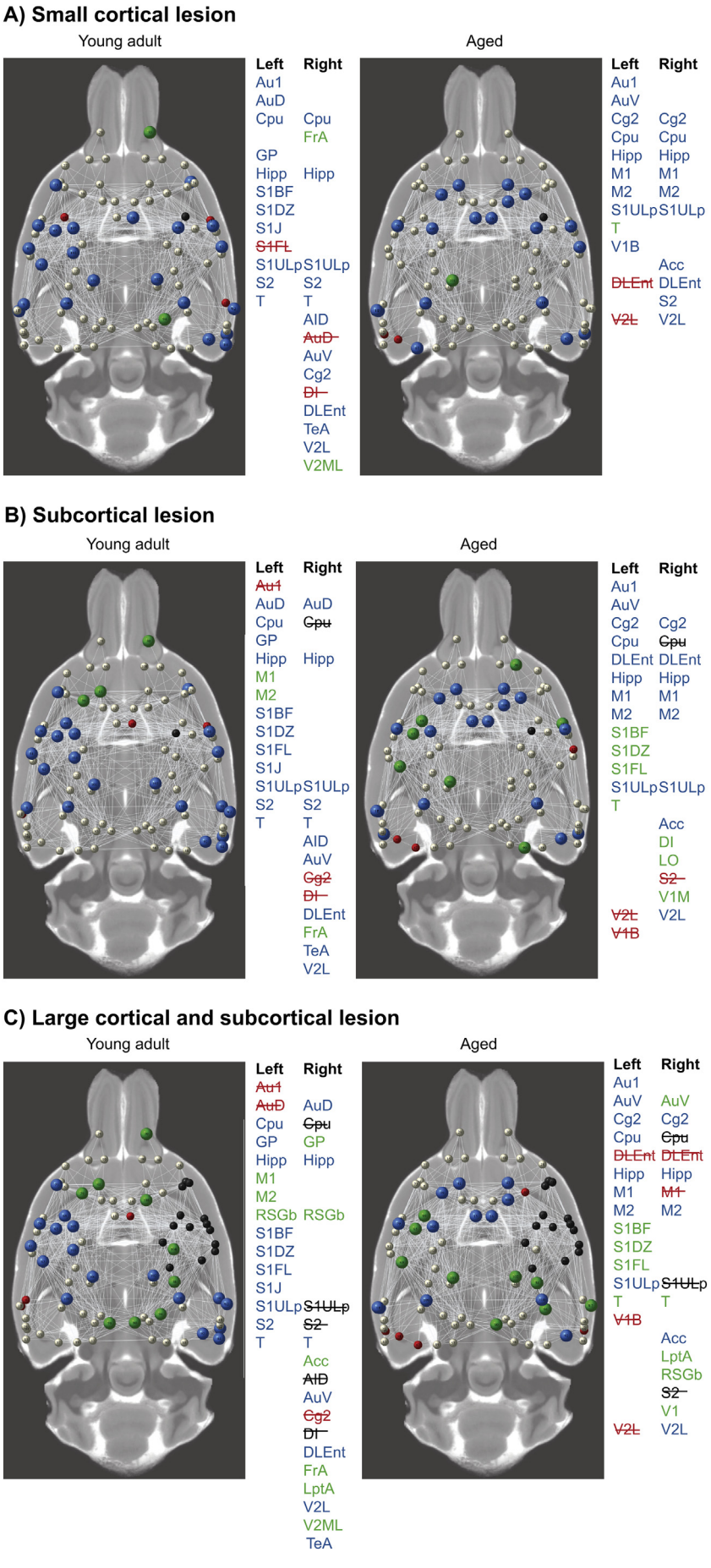

Fig. 5. Hub shifts in structural whole-brain networks after unilateral stroke lesion simulations in young adult and aged rat brain. Hub shifts are displayed after unilateral (right-sided) stroke lesion simulation in (A) a small cortical area, (B) a subcortical area, and (C) a large cortical and subcortical area. Hub nodes, overlaid on an axial structural MR image of a rat brain slice, are displayed in the 3D network as large nodes, whereas other (non-hub) regions are represented as small (white) nodes. Regions with maintained hub station after stroke lesion simulation are shown as large blue nodes, whereas regions that acquired a hub status are presented as large green nodes. Regions that lost hub status are presented as small red nodes. Lesioned nodes are presented in dark-grey colour. Networks are shown for young adult (left) and aged rats (right). Hub regions are listed right from the maps. Regions with acquired hub status are shown in green, and regions with lost hub status are crossed-out in red or black (lesioned nodes). (For interpretation of the references to colour in this figure legend, the reader is referred to the web version of this article.)

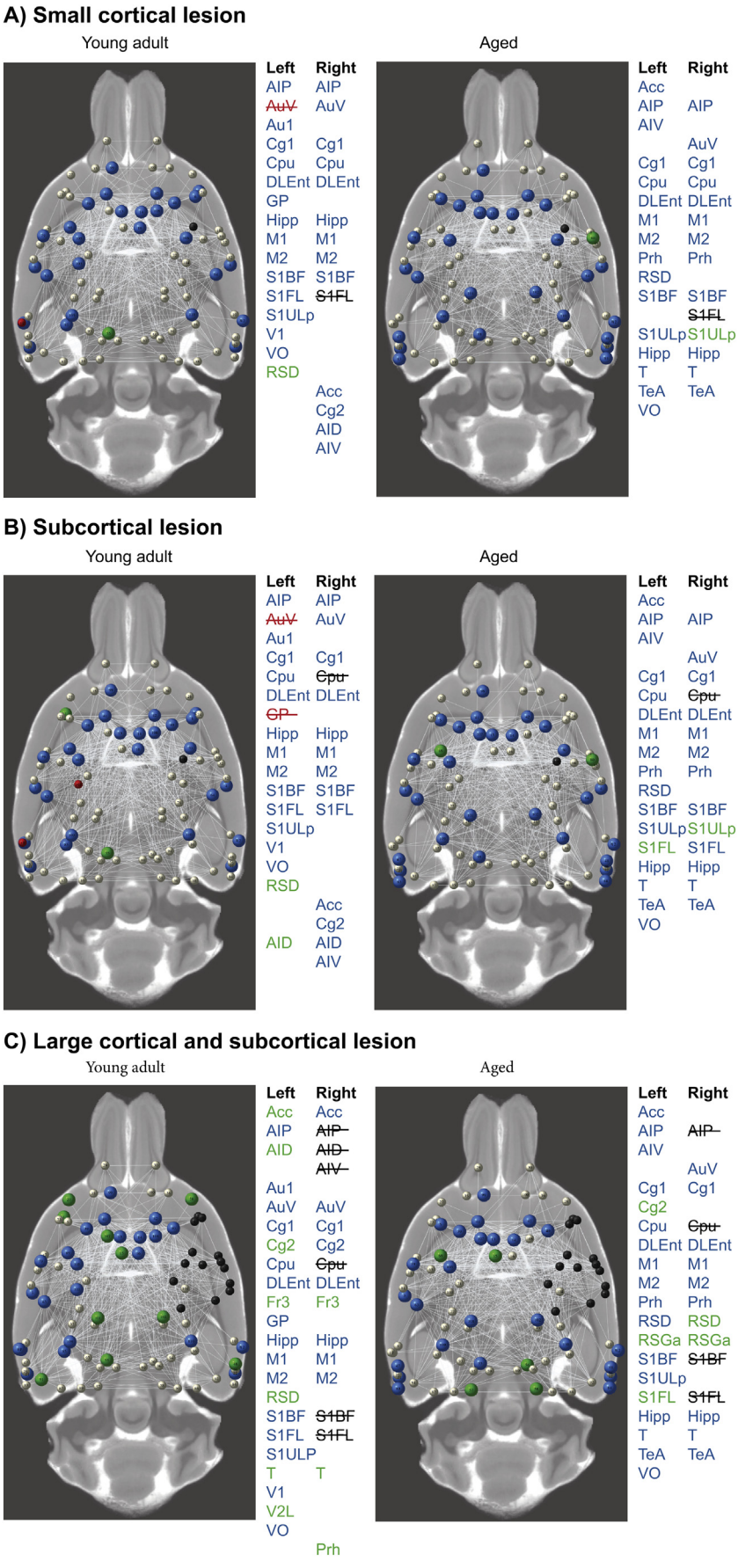

Fig. 6. Hub shifts in functional whole-brain networks after unilateral stroke lesion simulations in young adult and aged rat brain. Hub shifts are displayed after unilateral (right-sided) stroke lesion simulation in (A) a small cortical area, (B) a subcortical area and (C) a large cortical and subcortical area. Hub nodes, overlaid on an axial structural MR image of a rat brain slice, are displayed in the 3D network as large nodes, whereas other (non-hub) regions are represented as small (white) nodes. Regions with maintained hub status after stroke lesion simulation are shown as large blue nodes, whereas regions that acquired a hub status are presented as large green nodes. Regions that lost hub status are presented as small red nodes. Lesioned nodes are presented in dark-grey colour. Networks are shown for young adult (left) and aged rats (right). Hub regions are listed right from the maps. Regions with acquired hub status are shown in green, and regions with lost hub status are crossed-out in red or black (lesioned nodes). (For interpretation of the references to colour in this figure legend, the reader is referred to the web version of this article.)

Table 3
Dice coefficients (95% CI) for the overlap in hub regions before and after stroke simulations, in structural and functional brain networks of young adult and old rats.

	Structural network		*Functional network*	
	Young adult	*Aged*	*Young adult*	*Aged*
Cortical stroke	0.78 *(0.61–0.93)*	0.86 *(0.70–1.00)*	0.90 *(0.78–1.00)*	0.93 *(0.83–1.00)*
Subcortical stroke	0.71 *(0.54–0.88)*	0.61 *(0.42–0.79)*	0.84 *(0.70–0.96)*	0.90 *(0.79–1.00)*
Cortical plus subcortical stroke	0.47 *(0.30–0.64)*	0.44 *(0.26–0.62)*	0.55 *(0.39–0.71)*	0.71 *(0.55–0.85)*

lesion simulation study are largely in agreement with our previous in vivo resting-state fMRI study, in which we measured changes in the bilateral sensorimotor network after transient MCAO in young adult rats (van Meer et al., 2012). In both studies we found a longer path length and higher clustering coefficient in functional networks in response to stroke lesions in subcortical, or cortical plus subcortical tissue. The effects were considerably smaller when lesions were confined to only subcortical or cortical tissue, regardless whether this was a hub (i.e. hippocampus or CPu) or a non-hub region (i.e. medial parietal association cortex), which reflects robustness of the functional and structural networks against relatively small focal injury. Apparently, this was not affected by age, because the results were similar in young adult and aged rats.

Our stroke lesion simulations also resulted in clear shifts of hub regions in the structural and functional networks. Network hub regions are believed to be key players in the outcome of brain disorders (Crossley et al., 2014; Stam, 2014). Hub damage may have severe consequences for network function, while hub shifts may contribute to network remodeling. In our study, the number of hub shifts was higher in structural than in functional networks, which we observed in young adult as well as old rats. We speculate that this relates to the dependency of functional connectivity on direct as well as indirect structural connections (Adachi et al., 2012; Honey et al., 2009), which may facilitate network resilience. Since we only removed nodes and their direct connections in our lesion simulations, diffusion-based structural networks, which in essence only contain direct connections, would be more severely affected.

The lesion-induced hub shifts were different between young adult and aged rats. In aged rats contralesional somatosensory areas acquired hub status after subcortical or cortical plus subcortical stroke lesion simulations, which was not observed in young adult rats. This may relate to enhanced neural activity or functional connectivity in the contralesional hemisphere, which has been measured in stroke patients and animal models (Grefkes and Fink, 2014; van Meer et al., 2010a, 2010b). Why increased involvement of contralesional sensorimotor areas after unilateral stroke appeared more specifically in aged brain in our simulation study, and whether it may lead to worsening of functional outcome or contribute to functional recovery, remains to be elucidated. The local differences in structural and functional brain networks, including hub regions, between healthy young adult and aged rats, may have contributed to the different effects of lesion simulations between the two age groups. This underlines the critical role of age in the outcome of preclinical stroke studies in animal models, which often only involve young adult rodents, thereby limiting bench-to-bedside translation (Dirnagl, 2016).

It is important to realize that our computational simulation study only assessed direct effects of lesions on network status by elimination of nodes. Dynamic network responses, such as subsequent degeneration or regeneration, which can strongly depend on age (Betzel et al., 2014; Damoiseaux, 2017; Wang et al., 2015; Burke and Barnes, 2006; Niccoli and Partridge, 2012), were not accounted for. Another limitation is the use of anesthesia during resting-state fMRI, which is known to affect functional connectivity measurements (Paasonen et al., 2018). However, it might be argued that functional connectivity in anesthetized animals better reflects 'resting state' (i.e. baseline) connectivity than functional connectivity under awake conditions, which may be significantly affected by stress and motion. We used the same anesthesia protocol for all developmental stages, which enabled us to compare age effects under the same conditions. Nevertheless, future studies should look into (differences in) effects of anesthesia on network parameters across the lifespan and after stroke.

A limitation of diffusion-based tractography for structural connectivity measurement, is that white matter tracts are reconstructed from the underlying diffusion profiles, with limited power to resolve complex fiber configurations (e.g. crossing, bending and fanning fibers). This can result in considerable amounts of false positive and false negative connections (Calabrese et al., 2015; Jeurissen et al., 2017; Sinke et al., 2018; Thomas et al., 2014). Nevertheless, diffusion-based tractography is currently the only method to map whole-brain structural connections in vivo at the macro-scale. For our study we used a state-of-the-art approach, combining CSD-based tractography – which partially accounts for crossing fibers – with whole-brain filtering of tracts, which has been shown to yield biologically accurate connectomes (Smith et al., 2015, 2013).

Future research involving longitudinal in vivo imaging studies and improved structural and functional connectivity reconstruction algorithms combined with advanced network analysis strategies may provide further insights in the causes and consequences of age-related differences in susceptibility and resilience to stroke injury. In the end, knowledge of the structural and functional network status of a stroke patient's brain, could guide selection of appropriate recovery-enhancing treatment strategies targeted at optimal engagement of a patient's intact neural circuitry.

In conclusion, our study showed that global structural and functional network features are largely similar in young adult and old aged rat brains, and respond comparably to different types of stroke simulations. On the other hand, local network differences, particularly reflected by shifts in hub nodes, were identified between the brains of young adult and aged rats, before and after simulated stroke. These age-dependent neural network changes may play a critical role in the vulnerability and resilience to (stroke-induced) brain injury.

Funding

This work was supported by the Netherlands Organization for Scientific Research (NWO-VICI 016.130.662; NWO-VENI 016.168.038), and the Dutch Brain Foundation [F2014(1)-06].

Declaration of interest

None.

Appendix A. Supplementary data

Supplementary data to this article can be found online at https://doi.org/10.1016/j.nbd.2018.08.003.

References

Achard, S., Bullmore, E., 2007. Efficiency and cost of economical brain functional networks. PLoS Comput. Biol. 3, 0174–0183. https://doi.org/10.1371/journal.pcbi.0030017.

Adachi, Y., Osada, T., Sporns, O., Watanabe, T., Matsui, T., Miyamoto, K., Miyashita, Y., 2012. Functional connectivity between anatomically unconnected areas is shaped by collective network-level effects in the macaque cortex. Cereb. Cortex 22, 1586–1592. https://doi.org/10.1093/cercor/bhr234.

Aerts, H., Fias, W., Caeyenberghs, K., Marinazzo, D., 2016. Brain networks under attack:

Robustness properties and the impact of lesions. Brain 139, 3063–3083. https://doi.org/10.1093/brain/aww194.
Agcaoglu, O., Miller, R., Mayer, A., Hugdahl, K., Calhoun, V., 2015. Lateralization of resting state networks and relationship to age and gender. NeuroImage 104, 310–325. https://doi.org/10.1016/j.neuroimage.2014.09.001.
Altman, D.G., Bland, J.M., 2011. How to obtain the P value from a confidence interval. BMJ 343, d2304. https://doi.org/10.1136/bmj.d2304.
Andersson, J.L.R., Sotiropoulos, S.N., 2016. An integrated approach to correction for off-resonance effects and subject movement in diffusion MR imaging. NeuroImage 125, 1063–1078. https://doi.org/10.1016/j.neuroimage.2015.10.019.
Andersson, J.L.R., Jenkinson, M., Smith, S., 2007. Non-linear registration, aka spatial normalisation. FMRIB Technial Report TR07JA2. In: Oxford Centre for Functional Magnetic Resonance Imaging of the Brain. Department of Clinical Neurology, Oxford University, Oxford, UK.
Balls, M., Goldberg, A., Fentem, J.H., Broadhead, C., Bursch, R., Festing, M., Frazier, J., Hendriksen, F., Jennings, M., van der Kamp, M., Morton, D., Rowan, A., Russell, C., Russell, W., Spielmann, H., Stephens, M., Stokes, W., Straughan, D., Yager, J., Zurlo, J., van Zuphen, B., 1995. The three Rs: the way forward. Altern. to Lab. Anim. ATLA 23, 838–866.
Barrat, A., Barthélemy, M., Pastor-Satorras, R., Vespignani, A., 2004. The architecture of complex weighted networks. Proc. Natl. Acad. Sci. U. S. A. 101, 3747–3752. https://doi.org/10.1073/pnas.0400087101.
Bassett, D.S., Bullmore, E.T., 2009. Human brain networks in health and disease. Curr. Opin. Neurlogy 22, 340–347. https://doi.org/10.1097/WCO.0b013e32832d93dd.
Bassett, D.S., Sporns, O., 2017. Network neuroscience. Nat. Neurosci. 20, 353–364. https://doi.org/10.1038/nn.4502.
Benjamini, Y., Hochberg, Y., 1995. Controlling the false discovery rate : a practical and powerful approach to multiple testing. J. R. Stat. Soc. Ser. B 57, 289–300.
Betzel, R.F., Byrge, L., He, Y., Goni, J., Zuo, X.N., Sporns, O., 2014. Changes in structural and functional connectivity among resting-state networks across the human lifespan. NeuroImage 102, 345–357. https://doi.org/10.1016/j.neuroimage.2014.07.067.
Biernaskie, J., Corbett, D., 2001. Enriched rehabilitative training promotes improved forelimb motor function and enhanced dendritic growth after focal ischemic injury. J. Neurosci. 21, 5272–5280. https://doi.org/10.1523/JNEUROSCI.21-14-05272.2001.
Bland, J.M., Altman, D.G., 2015. Statistics notes: Bootstrap resampling methods. BMJ 350, h2622. https://doi.org/10.1136/bmj.h2622.
Blockx, I., Van Camp, N., Verhoye, M., Boisgard, R., Dubois, A., Jego, B., Jonckers, E., Raber, K., Siquier, K., Kuhnast, B., Dollé, F., Nguyen, H.P., Von Hörsten, S., Tavitian, B., Van der Linden, A., 2011. Genotype specific age related changes in a transgenic rat model of Huntington's disease. NeuroImage 58, 1006–1016. https://doi.org/10.1016/j.neuroimage.2011.07.007.
Brandes, U., 2001. A Faster Algorithm for Betweenness Centrality. J. Math. Sociol. 25, 163–177.
Bullmore, E., Sporns, O., 2009. Complex brain networks: graph theoretical analysis of structural and functional systems. Nat. Rev. Neurosci. 10, 186–198. https://doi.org/10.1038/nrn2575.
Burke, S.N., Barnes, C.A., 2006. Neural plasticity in the ageing brain. Nat. Rev. Neurosci. 7, 30–40. https://doi.org/10.1038/nrn1809.
Cai, J., Ji, Q., Xin, R., Zhang, D., Na, X., Peng, R., Li, K., 2016. Contralesional cortical structural reorganization contributes to motor recovery after sub-cortical stroke: a longitudinal voxel-based morphometry study. Front. Hum. Neurosci. 10, 393. https://doi.org/10.3389/fnhum.2016.00393.
Calabrese, E., Badea, A., Cofer, G., Qi, Y., Johnson, G.A., 2015. A diffusion MRI tractography connectome of the mouse brain and comparison with neuronal tracer data. Cereb. Cortex 1–10. https://doi.org/10.1093/cercor/bhv121.
Carter, A.R., Shulman, G.L., Corbetta, M., 2012. Why use a connectivity-based approach to study stroke and recovery of function? NeuroImage 62, 2271–2280. https://doi.org/10.1016/j.neuroimage.2012.02.070.
Cox, R.W., 1996. AFNI: software for analysis and visualization of functional magnetic resonance neuroimages. Comput. Biomed. Res. 29, 162–173.
Cramer, S.C., 2008. Repairing the human brain after stroke: I. Mechanisms of spontaneous recovery. Ann. Neurol. 63, 272–287. https://doi.org/10.1002/ana.21393.
Crofts, J.J., Higham, D.J., Bosnell, R., Jbabdi, S., Matthews, P.M., Behrens, T.E.J., Johansen-Berg, H., 2011. Network analysis detects changes in the contralesional hemisphere following stroke. NeuroImage 54, 161–169. https://doi.org/10.1016/j.neuroimage.2010.08.032.
Crossley, N.A., Mechelli, A., Scott, J., Carletti, F., Fox, P.T., McGuire, P., Bullmore, E.T., 2014. The hubs of the human connectome are generally implicated in the anatomy of brain disorders. Brain 137, 2382–2395. https://doi.org/10.1093/brain/awu132.
Dacosta-Aguayo, R., Graña, M., Fernández-Andújar, M., López-Cancio, E., Cáceres, C., Bargalló, N., Barrios, M., Clemente, I., Monserrat, P.T., Sas, M.A., Dávalos, A., Auer, T., Mataró, M., 2014. Structural integrity of the contralesional hemisphere predicts cognitive impairment in ischemic stroke at three months. PLoS One 9, e86119. https://doi.org/10.1371/journal.pone.0086119.
Damoiseaux, J.S., 2017. Effects of Aging on Functional and Structural Brain Connectivity. NeuroImage 160, 32–40. https://doi.org/10.1016/j.neuroimage.2017.01.077.
van den Heuvel, M.P., Mandl, R.C.W., Stam, C.J., Kahn, R.S., Hulshoff Pol, H.E., 2010. Aberrant frontal and temporal complex network structure in schizophrenia: a graph theoretical analysis. J. Neurosci. 30, 15915–15926. https://doi.org/10.1523/JNEUROSCI.2874-10.2010.
van den Heuvel, M.P., de Reus, M.A., Feldman Barrett, L., Scholtens, L.H., Coopmans, F.M.T., Schmidt, R., Preuss, T.M., Rilling, J.K., Li, L., 2015. Comparison of diffusion tractography and tract-tracing measures of connectivity strength in rhesus macaque connectome. Hum. Brain Mapp. 36, 3064–3075. https://doi.org/10.1002/hbm.22828.
van den Heuvel, M.P., Bullmore, E.T., Sporns, O., 2016a. Comparative connectomics. Trends Cogn. Sci. 20, 345–361. https://doi.org/10.1016/j.tics.2016.03.001.
van den Heuvel, M.P., Scholtens, L.H., de Reus, M.A., 2016b. Topological organization of connectivity strength in the rat connectome. Brain Struct. Funct. 221, 1719–1736. https://doi.org/10.1007/s00429-015-0999-6.
Dijkstra, E.W., 1959. A note on two probles in connexion with graphs. Numer. Math. 1, 269–271. https://doi.org/10.1007/BF01386390.
Dirnagl, U., 2016. Thomas Willis lecture: Is translational stroke research broken, and if so, how can we fix it? Stroke 47, 2148–2153. https://doi.org/10.1161/STROKEAHA.116.013244.
Fagiolo, G., 2007. Clustering in Complex Directed Networks. Phys. Rev. 76 (76), 026107. https://doi.org/10.1103/PhysRevE.76.026107.
Feigin, V.L., Forouzanfar, M.H., Krishnamurthi, R., Mensah, G.A., Connor, M., Bennett, D.A., Moran, A.E., Sacco, R.L., Anderson, L., Truelsen, T., O'Donnell, M., Venketasubramanian, N., Barker-Collo, S., Lawes, C.M.M., Wang, W., Shinohara, Y., Witt, E., Ezzati, M., Naghavi, M., Murray, C., 2014. Global Burden of Diseases, Injuries, and R.F.S. 2010 (GBD 2010) and the G.S.E.G., 2014. Global and regional burden of stroke during 1990–2010: findings from the Global Burden of Disease Study 2010. Lancet 383, 245–254. https://doi.org/10.1016/S0140-6736(13)61953-4.
Fluri, F., Schuhmann, M.K., Kleinschnitz, C., 2015. Animal models of ischemic stroke and their application in clinical research. Drug Des. Devel. Ther. 9, 3445–3454. https://doi.org/10.2147/DDDT.S56071.
Freeman, L.C., 1977. A set of measures of centrality based on betweenness. Sociometry 40, 35–41.
Garcia, J.H., Liu, K.-F., Ho, K.-L., 1995. Neuronal necrosis after middle cerebral artery occlusion in wistar rats progresses at different time intervals in the caudoputamen and the cortex. Stroke 26, 636–643. https://doi.org/10.1161/01.STR.26.4.636.
Gong, G., Rosa-Neto, P., Carbonell, F., Chen, Z.J., He, Y., Evans, A.C., 2009. Age- and gender-related differences in the cortical anatomical network. J. Neurosci. 29, 15684–15693. https://doi.org/10.1523/JNEUROSCI.2308-09.2009.
Granziera, C., Ay, H., Koniak, S.P., Krueger, G., Sorensen, A.G., 2012. Diffusion tensor imaging shows structural remodeling of stroke mirror region: results from a pilot study. Eur. Neurol. 67, 370–376. https://doi.org/10.1159/000336062.
Gratton, C., Nomura, E.M., Pérez, F., D'Esposito, M., 2012. Focal brain lesions to critical locations cause widespread disruption of the modular organization of the brain. J. Cogn. Neurosci. 24, 1275–1285. https://doi.org/10.1162/jocn_a_00222.
Grefkes, C., Fink, G.R., 2011. Reorganization of cerebral networks after stroke: new insights from neuroimaging with connectivity approaches. Brain 134, 1264–1276. https://doi.org/10.1093/brain/awr033.
Grefkes, C., Fink, G.R., 2014. Connectivity-based approaches in stroke and recovery of function. Lancet Neurol. 13, 206–216. https://doi.org/10.1016/S1474-4422(13)70264-3.
Herson, P.S., Traystman, R.J., 2014. Animal models of stroke: translational potential at present and in 2050. Future Neurol. 9, 541–551. https://doi.org/10.2217/fnl.14.44.
Honey, C.J., Sporns, O., Cammoun, L., Gigandet, X., Thiran, J.P., Meuli, R., Hagmann, P., 2009. Predicting human resting-state functional connectivity from structural connectivity. Proc. Natl. Acad. Sci. U. S. A. 106, 2035–2040. https://doi.org/10.1073/pnas.0811168106.
Humphries, M.D., Gurney, K., 2008. Network 'small-world-ness ': a quantitative method for determining canonical network equivalence. PLoS One 3, e0002051. https://doi.org/10.1371/journal.pone.0002051.
Jenkinson, M., Smith, S., 2001. A global optimisation method for robust affine registration of brain images. Med. Image Anal. 5, 143–156. https://doi.org/10.1016/S1361-8415(01)00036-6.
Jenkinson, M., Bannister, P., Brady, M., Smith, S., 2002. Improved optimization for the robust and accurate linear registration and motion correction of brain images. NeuroImage 17, 825–841. https://doi.org/10.1006/nimg.2002.1132.
Jenkinson, M., Beckmann, C.F., Behrens, T.E.J., Woolrich, M.W., Smith, S.M., 2012. Fsl. *Neuroimage* 62, 782–790. https://doi.org/10.1016/j.neuroimage.2011.09.015.
Jeurissen, B., Tournier, J.-D., Dhollander, T., Connelly, A., Sijbers, J., 2014. Multi-tissue constrained spherical deconvolution for improved analysis of multi-shell diffusion MRI data. NeuroImage 103, 411–426. https://doi.org/10.1016/j.neuroimage.2014.07.061.
Jeurissen, B., Descoteaux, M., Mori, S., Leemans, A., 2017. Diffusion MRI fiber tractography of the brain. NMR Biomed., e3785. https://doi.org/10.1002/nbm.3785.
Jiang, L., Xu, H., Yu, C., 2013. Brain connectivity plasticity in the motor network after ischemic stroke. Neural Plast. 2013, 1–11. https://doi.org/10.1155/2013/924192.
Johansen-Berg, H., Scholz, J., Stagg, C.J., 2010. Relevance of structural brain connectivity to learning and recovery from stroke. Front. Syst. Neurosci. 4, 146. https://doi.org/10.3389/fnsys.2010.00146.
Jones, T.A., 2017. Motor compensation and its effects on neural reorganization after stroke. Nat. Rev. Neurosci. 18, 267–280. https://doi.org/10.1038/nrn.2017.26.
Jones, T.A., Kleim, J.A., Greenough, W.T., 1996. Synaptogenesis and dendritic growth in the cortex opposite unilateral sensorimotor cortex damage in adult rats: a quantitative electron microscopic examination. Brain Res. 733, 142–148. https://doi.org/10.1016/S0006-8993(96)00792-5.
Li, Y., Chopp, M., Jiang, N., Zhang, Z.G., Zaloga, C., 1995. Induction of DNA fragmentation after 10 to 120 mi of focal cerebral ischemia in rats. Stroke 26, 1252–1258. https://doi.org/10.1161/01.STR.26.7.1252.
Liang, A.C., Mandeville, E.T., Maki, T., Shindo, A., Som, A.T., Egawa, N., Itoh, K., Chuang, T.T., McNeish, J.D., Holder, J.C., Lok, J., Lo, E.H., Arai, K., 2016. Effects of aging on neural stem/progenitor cells and oligodendrocyte precursor cells after focal cerebral ischemia in spontaneously hypertensive rats. Cell Transplant. 25, 705–714. https://doi.org/10.3727/096368916X690557.
Liu, F., Yuan, R., Benashski, S.E., McCullough, L.D., 2009. Changes in experimental stroke outcome across the lifespan. J. Cereb. Blood Flow Metab. 29, 792–802. https://doi.

org/10.1038/jcbfm.2009.5.
Longa, E.Z., Weinstein, P.R., Carlson, S., Cummins, R., 1989. Reversible middle cerebral artery occlusion without craniectomy in rats. Stroke 20, 84–91. https://doi.org/10.1161/01.STR.20.1.84.
Majka, P., Kublik, E., Furga, G., Wójcik, D.K., 2012. Common atlas format and 3D brain atlas reconstructor: infrastructure for constructing 3D brain atlases. Neuroinformatics 10, 181–197. https://doi.org/10.1007/s12021-011-9138-6.
Maslov, S., Sneppen, K., 2002. Specificity and stability in topology of protein networks. Science 80 (296), 910–914.
van Meer, M.P.A., van der Marel, K., Otte, W.M., Berkelbach van der Sprenkel, J.W., Dijkhuizen, R.M., van der Sprenkel, B., Willem, J., 2010a. Correspondence between altered functional and structural connectivity in the contralesional sensorimotor cortex after unilateral stroke in rats: a combined resting-state functional MRI and manganese-enhanced MRI study. J. Cereb. Blood Flow Metab. 30, 1707–1711. https://doi.org/10.1038/jcbfm.2010.124.
van Meer, M.P.A., van der Marel, K., Wang, K., Otte, W.M., el Bouazati, S., Roeling, T.A.P., Viergever, M.A., Berkelbach van der Sprenkel, J.W., Dijkhuizen, R.M., 2010b. Recovery of sensorimotor function after experimental stroke correlates with restoration of resting-state interhemispheric functional connectivity. J. Neurosci. 30, 3964–3972. https://doi.org/10.1523/JNEUROSCI.5709-09.2010.
van Meer, M.P.A., Otte, W.M., van der Marel, K., Nijboer, C.H., Kavelaars, A., van der Sprenkel, J.W.B., Viergever, M.A., Dijkhuizen, R.M., 2012. Extent of bilateral neuronal network reorganization and functional recovery in relation to stroke severity. J. Neurosci. 32, 4495–4507. https://doi.org/10.1523/JNEUROSCI.3662-11.2012.
Meier-Ruge, W., Ulrich, J., Brühlmann, M., Meier, E., 1992. Age-related white matter atrophy in the human brain. Ann. N. Y. Acad. Sci. 673, 260–269. https://doi.org/10.1111/j.1749-6632.1992.tb27462.x.
Mengler, L., Khmelinskii, A., Diedenhofen, M., Po, C., Staring, M., Lelieveldt, B.P.F., Hoehn, M., 2014. Brain maturation of the adolescent rat cortex and striatum: changes in volume and myelination. NeuroImage 84, 35–44. https://doi.org/10.1016/j.neuroimage.2013.08.034.
Meunier, D., Achard, S., Morcom, A., Bullmore, E., 2009. Age-related changes in modular organization of human brain functional networks. NeuroImage 44, 715–723. https://doi.org/10.1016/j.neuroimage.2008.09.062.
Murphy, T.H., Corbett, D., 2009. Plasticity during stroke recovery: from synapse to behaviour. Nat. Rev. Neurosci. 10, 861–872. https://doi.org/10.1038/nrn2735.
Newman, M.E.J., 2003. The structure and function of complex networks. Soc. Ind. Appl. Math. Rev. 45, 167–256.
Niccoli, T., Partridge, L., 2012. Ageing as a risk factor for disease. Curr. Biol. 22, R741–R752. https://doi.org/10.1016/j.cub.2012.07.024.
Paasonen, J., Stenroos, P., Salo, R.A., Kiviniemi, V., Gröhn, O., 2018. Functional connectivity under six anesthesia protocols and the awake condition in rat brain. NeuroImage 172, 9–20. https://doi.org/10.1016/j.neuroimage.2018.01.014.
Paxinos, G., Watson, W., 2005. The Rat Brain in Stereotaxic Coordinates, 5th edition. Elsevier Academic Press, Amsterdam.
Rehme, A.K., Grefkes, C., 2013. Cerebral network disorders after stroke: evidence from imaging-based connectivity analyses of active and resting brain states in humans. J. Physiol. 591, 17–31. https://doi.org/10.1113/jphysiol.2012.243469.
Sala-Llonch, R., Junqué, C., Arenaza-Urquijo, E.M., Vidal-Piñeiro, D., Valls-Pedret, C., Palacios, E.M., Domènech, S., Salvà, A., Bargalló, N., Bartrés-Faz, D., 2014. Changes in whole-brain functional networks and memory performance in aging. Neurobiol. Aging 35, 2193–2202. https://doi.org/10.1016/j.neurobiolaging.2014.04.007.
Salat, D.H., Tuch, D.S., Greve, D.N., Van Der Kouwe, A.J.W., Hevelone, N.D., Zaleta, A.K., Rosen, B.R., Fischl, B., Corkin, S., Diana Rosas, H., Dale, A.M., 2005. Age-related alterations in white matter microstructure measured by diffusion tensor imaging. Neurobiol. Aging 26, 1215–1227. https://doi.org/10.1016/j.neurobiolaging.2004.09.017.
Schaechter, J.D., Fricker, Z.P., Perdue, K.L., Helmer, K.G., Vangel, M.G., Greve, D.N., Makris, N., 2009. Microstructural status of ipsilesional and contralesional corticospinal tract correlates with motor skill in chronic stroke patients. Hum. Brain Mapp. 30, 3461–3474. https://doi.org/10.1002/hbm.20770.
Sinke, M.R.T., Otte, W.M., Christiaens, D., Schmitt, O., Leemans, A., van der Toorn, A., Sarabdjitsingh, R.A., Joëls, M., Dijkhuizen, R.M., 2018. Diffusion MRI-based cortical connectome reconstruction: dependency on tractography procedures and neuroanatomical characteristics. Brain Struct. Funct. 223, 2269–2285. https://doi.org/10.1007/s00429-018-1628-y.
Smith, S.M., 2002. Fast robust automated brain extraction. Hum. Brain Mapp. 17, 143–155. https://doi.org/10.1002/hbm.10062.
Smith, R.E., Tournier, J.D., Calamante, F., Connelly, A., 2013. SIFT: spherical-deconvolution informed filtering of tractograms. NeuroImage 67, 298–312. https://doi.org/10.1016/j.neuroimage.2012.11.049.
Smith, R.E., Tournier, J.D., Calamante, F., Connelly, A., 2015. The effects of SIFT on the reproducibility and biological accuracy of the structural connectome. NeuroImage 104, 253–265. https://doi.org/10.1016/j.neuroimage.2014.10.004.
Sporns, O., 2010. Networks of the Brain. MIT Press.
Sporns, O., Honey, C.J., Kötter, R., 2007. Identification and classification of hubs in brain networks. PLoS One 2, e1049. https://doi.org/10.1371/journal.pone.0001049.
Stam, C.J., 2014. Modern network science of neurological disorders. Nat. Rev. Neurosci. 15, 683–695. https://doi.org/10.1038/nrn3801.
Stam, C.J., De Haan, W., Daffertshofer, A., Jones, B.F., Manshanden, I., Van Walsum, A.M.V.C., Montez, T., Verbunt, J.P.A., De Munck, J.C., Van Dijk, B.W., Berendse, H.W., Scheltens, P., 2009. Graph theoretical analysis of magnetoencephalographic functional connectivity in Alzheimer's disease. Brain 132, 213–224. https://doi.org/10.1093/brain/awn262.
Stroemer, R.P., Kent, T.A., Hulsebosch, C.E., 1995. Neocortical neural sprouting, synaptogensis, and behavioral recovery after neocortical infarction in rats. Stroke 26, 2135–2144. https://doi.org/10.1161/01.STR.26.11.2135.
Thomas, C., Ye, F.Q., Irfanoglu, M.O., Modi, P., Saleem, K.S., Leopold, D.A., Pierpaoli, C., 2014. Anatomical accuracy of brain connections derived from diffusion MRI tractography is inherently limited. Proc. Natl. Acad. Sci. U. S. A. 111, 16574–16579. https://doi.org/10.1073/pnas.1405672111.
Tournier, J.D., Calamante, F., Connelly, A., 2010. Improved probabilistic streamlines tractography by 2nd order integration over fibre orientation distributions. Proc. Int. Soc. Magn. Reson. Med. 1670.
Tournier, J.D., Calamante, F., Connelly, A., 2012. MRtrix: diffusion tractography in crossing fiber regions. Int. J. Imaging Syst. Technol. 22, 53–66. https://doi.org/10.1002/ima.22005.
Wang, L., Li, Y., Metzak, P., He, Y., Woodward, T.S., 2010. Age-related changes in topological patterns of large-scale brain functional networks during memory encoding and recognition. NeuroImage 50, 862–872. https://doi.org/10.1016/j.neuroimage.2010.01.044.
Wang, Z., Dai, Z., Gong, G., Zhou, C., He, Y., 2015. Understanding structural-functional relationships in the human brain. Neuroscience 21, 290–305. https://doi.org/10.1177/1073858414537560.
Watson, B.D., Dietrich, W.D., Busto, R., Wachtel, M.S., Ginsberg, M.D., 1985. Induction of reproducible brain infarction by photochemically initiated thrombosis. Ann. Neurol. 17, 497–504. https://doi.org/10.1002/ana.410170513.
Wu, K., Taki, Y., Sato, K., Kinomura, S., Goto, R., Okada, K., Kawashima, R., He, Y., Evans, A.C., Fukuda, H., 2012. Age-related changes in topological organization of structural brain networks in healthy individuals. Hum. Brain Mapp. 33, 552–568. https://doi.org/10.1002/hbm.21232.
Yin, Y., Yasuda, K., 2006. Similarity coefficient methods applied to the cell formation problem: a taxonomy and review. Int. J. Prod. Econ. 101, 329–352. https://doi.org/10.1016/j.ijpe.2005.01.014.
Zhang, W., Yang, S., Li, C., Chen, L., Tang, Y., 2009. Stereological investigation of age-related changes of myelinated fibers in the rat cortex. J. Neurosci. Res. 87, 2872–2880. https://doi.org/10.1002/jnr.22114.
Zhu, W., Wen, W., He, Y., Xia, A., Anstey, K.J., Sachdev, P., 2012. Changing topological patterns in normal aging using large-scale structural networks. Neurobiol. Aging 33, 899–913. https://doi.org/10.1016/j.neurobiolaging.2010.06.022.
Zuo, X.-N., Kelly, C., Di Martino, A., Mennes, M., Margulies, D.S., Bangaru, S., Grzadzinski, R., Evans, A.C., Zang, Y., Castellanos, X., Milham, M.P., 2010. Growing together and growing apart: regional and sex differences in the lifespan developmental trajectories of functional homotopy. J. Neurosci. 30, 15034–15043. https://doi.org/10.1523/JNEUROSCI.2612-10.2010.